ENHANCED SENSITIVITY OF SURFACE PLASMON RESONANCE SENSOR BASED ON COMBINATION OF Au/PEDOT:PSS NANOLAYERS

Nguyen Van Sau[a], Ma Thai Hoa[b], Nguyen Xuan Thi Diem Trinh[b], Nguyen Tan Tai[c*]

[a]School of Basic Science, Tra Vinh University, Tra Vinh, Vietnam
[b]Department of Activated Polymer and Nano Materials Applications, School of Applied Chemistry, Tra Vinh University, Tra Vinh, Vietnam
[c]Department of Materials Science, School of Applied Chemistry, Tra Vinh University, Tra Vinh, Vietnam
[*]Corresponding author: Email: nttai60@tvu.edu.vn

Article history
Received: September 24th, 2020
Received in revised form (1st): October 28th, 2020 | Received in revised form (2nd): November 3rd, 2020
Accepted: November 26th, 2020
Available online: February 5th, 2021

Abstract

This paper simulates an optical sensor utilizing a prism based on surface plasmon resonance (SPR). The simulations combine a layer of Au and an additional layer of different materials: aluminum arsenide (AlAs), poly(3,4-ethylenedioxythiophene) polystyrene sulfonate (PEDOT:PSS), zinc oxide (ZnO), and polydimethylsiloxane (PDMS) for SPR excitation. The simulations show that a sensor based on a combination of Au/PEDOT:PSS layers with thicknesses of 40 nm and 5 nm, respectively, offers a sensor sensitivity of 186.07°/RIU, which is 1.2 times better than that of a sensor using only a thin Au layer. The enhancement in sensor sensitivity offers advantages for early detection of small concentrations of bacteria in biomedical and chemical applications.

Keywords: Combination; Optical sensor; Sensitivity; Surface plasmon resonance.

DOI: http://dx.doi.org/10.37569/DalatUniversity.11.1.775(2021)

Loại bài báo: Bài báo nghiên cứu gốc có bình duyệt

1. INTRODUCTION

Nowadays, much research has been focused on the development of optical sensors based on surface plasmon resonance (SPR) for various applications in biomedicine and biochemistry for early diagnosis of diseases (Chien et al., 2007; Ho et al., 2002; Homola, 1995; Jorgenson & Yee, 1993; Nguyen et al., 2014; Nguyen et al., 2015; Nguyen et al., 2017; Telezhnikova & Homola, 2006; Truong et al., 2018; Van Gent et al., 1990; Wu et al., 2004; Yuan et al., 2007) and in environmental applications for detection of heavy metals (Chah et al., 2004; Fen et al., 2015; Palumbo et al., 2003; Panta et al., 2009). The SPR effect was first discovered by Andreas Otto, Kretschmann, and Raether using a prism with a thin metal coating (Otto, 1968; Raether & Kretschmann, 1968). Optical sensors utilizing SPR have been widely used for sensing applications, offering such advantages as label-free sensing and real-time monitoring (Maharana & Jha, 2012; Patnaik et al., 2015).

In the past few decades, many researchers have been working on theoretical and experimental investigations of optical sensors based on prisms or optical fibers operating at a single wavelength of 632.8 nm. Iga et al. (2004) investigated a sensing device based on a hetero-core structured fiber optic with a 50-nm thin silver film deposition. They used an LED with a wavelength of 680.0 nm to make an excitation of the SPR wave. The results showed that a sensitivity of 2.1×10^{-4} RIU was achieved with a refractive index operating range of 0.065 RIU. Vala et al. (2010) developed a novel compact SPR sensor based on a grating with a detection capability of up to 10 analytes with 10 independent fluid channels. The results show that a sensor resolution around 6.0×10^{-7} RIU was achieved. In addition, Turker and his coworkers used photodiodes to excite SPR waves in a grating coupler and obtained a sensitivity of around 10^{-7} RIU (Turker et al., 2011). In the same year, Yang and his coworkers studied an SPR sensor utilizing BK7 glass substrates based on the Kretschmann geometry. Bilayer films of SnO_2/Au were covered in glass substrates. The sensor was used to detect NO gas of 50 or 100 ppm (Yang et al., 2010). Later, Yuan et al. (2012) reported a theoretical investigation on two cascaded surface plasmon resonance fiber optic sensors. They used a combination of Au, Ag, and Ta_2O_5 for the SPR sensor. A sensor sensitivity around 6500 nm/RIU was obtained for the bilayer of Ta_2O_5 and Au (Yuan et al., 2012). Mishra et al. (2015) investigated an SPR sensor based on indium tin oxide (ITO) and silver (Ag) coated fibers for sensing in the visible regime. They demonstrated that the combination of ITO and Ag with a thickness of 80 nm and 40 nm, respectively, gives better detection accuracy than using a single material (ITO or Ag) (Mishra et al., 2015). In 2016, Zhao et al. (2016) demonstrated a surface plasmon resonance refractometer sensor based on side-polished single-mode optical fiber with Ag coating.

A sensor sensitivity up to 4,365.5 nm/RIU was achieved (Zhao et al., 2016). Srivastava et al. (2016) have reported the use of ITO for long-range SPR in combination with silicon dioxide, Teflon AF-1600, and Cytop. The established geometries were optimized to obtain a self-referenced sensing operation. The performance showed that the bilayer combination of Ag/ITO showed the best sensitivity with thicknesses of 46.7 nm and 250.0 nm, respectively. Akter and Razzak (2019) numerically demonstrated a plasmonic refractometer sensor using two-sided channels in both the visible and near-

infrared range. The photonic crystal fiber with a thin coating of the Au layer was characterized by using the finite element method. The sensor sensitivity of 5,000 nm/RIU with a sensor resolution of 2.0×10^{-5} RIU was achieved (Akter & Razzak, 2019). Most of the research has focused on the enhancement of the sensitivity of the optical sensor using visible wavelengths for SPR excitation and has achieved some good results. However, the use of those methods has some inherent drawbacks due to the low detection accuracy and sensor sensitivity, resulting in the limited detection of targets in small concentrations. An enhancement of the detection accuracy is associated with reproducibility, allowing reproducible experimental results. In addition, the penetration depth of the SPR wave in the sensing medium is also important for the sensor operation.

To date, several researchers have made theoretical studies on SPR sensors with multilayer compositions. They demonstrated that a coating layer consisting of bimetal nanoparticle composition was better than a monolayer in terms of the sensor figures of merit, such as the limit of detection, signal-to-noise ratio, sensitivity, and dynamic range of the sensing medium (Sharmal & Mohr, 2008).

In our work, the sensor sensitivity and detection accuracy are investigated based on a prism structure coated with a thin layer of Au in combination with an additional material, such as zinc oxide (ZnO), aluminum arsenide (AlAs), poly(3,4-ethylenedioxythiophene) polystyrene sulfonate (PEDOT: PSS), and polydimethylsiloxane (PDMS). The sensor is based on the Kretschmann configuration operating in the angle interrogation scheme. The angle modulation technique provides an accurate quantitative measurement of the refractive index of the targets, as the SPR angle is not affected by fluctuations of the light power source. In addition, the contribution of the imaginary part of the dielectric function of the additional layers (ZnO, AlAs, PEDOT:PSS, and PDMS) on the sensor performance was determined. Moreover, additional layers allow self-immobilization of proteins or peptides on the surface without a covalent cross-linker for biomedical applications. The sensor characteristics are investigated by changing the thicknesses of the Au and additional material layers with an operating wavelength of 633 nm given good repeatability with high detection accuracy. The present study will be useful in the fabrication of SPR sensors utilizing Au/additional layer structures for optimal performance.

2. MATERIALS AND METHODS

2.1. Sensor structure and materials for simulation

Figure 1 shows the sensor structure, which is composed of a thin Au layer and an additional layer (ZnO, AlAs, PEDOT:PSS, PDMS) with an excitation wavelength of 632.8 nm.

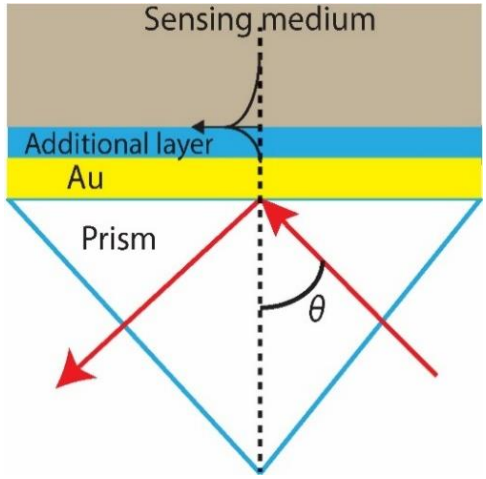

Figure 1. Structure of the SPR sensor

Dielectric constants used in the simulations of the BK7 prism, Au, and additional materials are given in Table 1.

Table 1. The dielectric constants of the materials

Materials	Wavelength (nm)	Dielectric constant ($\varepsilon_r + i\varepsilon_i$)	References
Prism (BK7)	632.8	2.28	Prabowo et al. (2018)
Au	632.8	-66.26 + 5.83i	McPeak et al. (2015)
ZnO	632.8	3.76	Stelling et al. (2017)
PEDOT:PSS	632.8	2.26 + 0.04i	Chen et al. (2015)
AlAs	632.8	8.64	Rakic and Majewski (1996)
PDMS	632.8	1.96	Gupta et al. (2019)

2.2. Transfer matrix method

In this work, the SPR excitation was based on a prism structure with a thin Au layer and an excitation wavelength of 632.8 nm. Laser light was used with the SPR sensors due to its high monochromatic light and lower adsorption by the sensing medium. The sensor structure of BK7/Au/additional layer/sensing medium was utilized in this simulation. The optimal thickness of the Au layer was estimated under the resonance condition versus reflected light. The thickness of the Au layer was varied from 30.0 nm to 55.0 nm with an increment of 5.0 nm due to the accuracy of the thermal evaporation system. The incoming light was directed at the prism/Au interface, and the incident angle was controlled from 0° to 90° to satisfy the resonant condition for excitation of the SPR wave. The transfer matrix method was used to calculate the reflectance by an angular modulation technique based on the Kretschmann sensor configuration with variable Au layer thicknesses. Using the transfer matrix method, the relations of the longitudinal modes of the electric and magnetic fields at the boundaries between two pairs of media, prism/Au and additional layer/sensing medium, are given below (Iga et al., 2004):

$$\begin{bmatrix} E_{t1} \\ H_{t1} \end{bmatrix} = M \begin{bmatrix} E_{t3} \\ H_{t3} \end{bmatrix} \tag{1}$$

where E_{t1}, $H_{t1,}$ E_{t3}, and H_{t3} are the longitudinal modes of the electric and magnetic fields at the boundary between the two media: the prism/Au and the additional layer/sensing medium, respectively. M is the transfer matrix, as given below:

$$M = \begin{bmatrix} M_{11} & M_{12} \\ M_{21} & M_{22} \end{bmatrix} \tag{2}$$

where,

$$M_{11} = \cos\beta_{Au}\cos\beta_{sem} - \frac{q_{sem}}{q_{Au}}\sin\beta_{Au}\sin\beta_{sem} \tag{3}$$

$$M_{12} = \frac{-i}{q_{sem}}\cos\beta_{Au}\sin\beta_{sem} - \frac{i}{q_{Au}}\sin\beta_{Au}\cos\beta_{sem} \tag{4}$$

$$M_{21} = -iq_{Au}\sin\beta_{Au}\cos\beta_{sem} - iq_{sem}\cos\beta_{Au}\sin\beta_{sem} \tag{5}$$

$$M_{22} = \frac{-q_{Au}}{q_{sem}}\sin\beta_{Au}\sin\beta_{sem} + \cos\beta_{Au}\cos\beta_{sem} \tag{6}$$

and

$$q_{Au} = \frac{(\varepsilon_{Au} - \varepsilon_{BK7}\sin^2\theta)^{1/2}}{\varepsilon_{Au}} \tag{7}$$

$$q_{sem} = \frac{(\varepsilon_{sem} - \varepsilon_{BK7}\sin^2\theta)^{1/2}}{\varepsilon_{sem}} \tag{8}$$

$$\beta_{Au} = \frac{2\pi d_{Au}}{\lambda}(\varepsilon_{Au} - \varepsilon_{BK7}\sin^2\theta)^{1/2} \tag{9}$$

$$\beta_{sem} = \frac{2\pi d_{sem}}{\lambda}(\varepsilon_{sem} - \varepsilon_{BK7}\sin^2\theta)^{1/2} \tag{10}$$

The reflection coefficient of the TM wave is given below

$$r_q = \frac{(M_{11} + M_{12}q_s) + q_{BK7} - (M_{21} + M_{22}q_s)}{(M_{11} + M_{12}q_s) + q_{BK7} + (M_{21} + M_{22}q_s)} \tag{11}$$

where

$$q_s = \frac{(\varepsilon_s - \varepsilon_{BK7} \sin^2 \theta)^{1/2}}{\varepsilon_s} \tag{12}$$

$$q_{BK7} = \frac{\cos\theta}{\sqrt{\varepsilon_{BK7}}} \tag{13}$$

The intensity of the reflected light is shown below

$$R = \left| r_p \right|^2 \tag{14}$$

where d_{Au} and d_{sem} are the thicknesses of the Au and additional materials, respectively. Parameters ε_{BK7}, ε_s, ε_{sem}, and ε_{Au} are the dielectric constants of the prism, the sensing medium, the additional materials, and the Au layer, respectively. θ is the incident angle and λ is the wavelength of the laser light.

3. RESULTS AND DISCUSSIONS

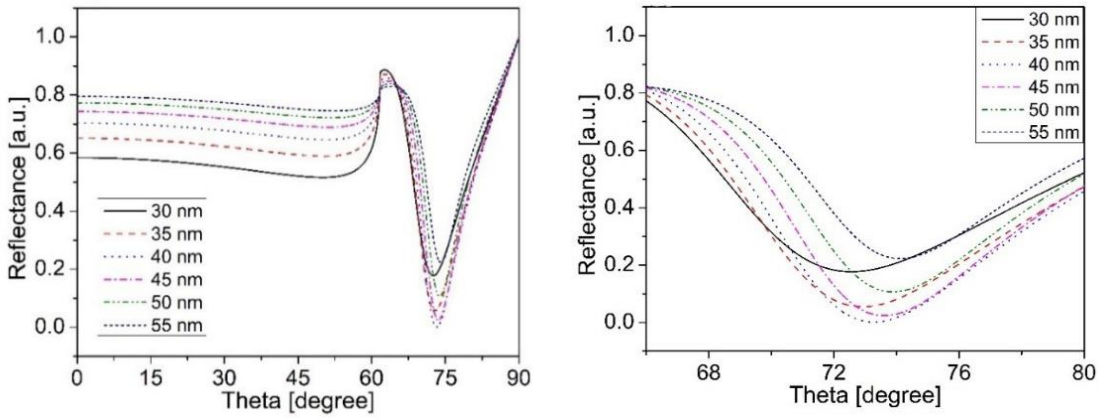

Figure 2. a) Simulated results for Au thicknesses from 30 nm to 55 nm for a wavelength of 633 nm; (b) Enlargement of (a) with a resonant angle range of 68°-80°

The results show that the resonance angle was slightly shifted from 72° to 73° based on the change in the Au layer thickness in the range from 30 nm to 55 nm, as shown in Figure 2(a). An increment of the Au thickness caused changes in reflectivity. When the thickness of the Au layer was around 40 nm, the reflectance reached a minimum value due to the strong coupling between the TM wave and the surface plasmon wave, as seen in Figure 2(b). When the thickness of the Au layer was larger or smaller than 40 nm, the reflectance decreased. The change in the thickness of the Au layer caused a change in the resonance condition and an increase in reflectance. Based on these results, it is worthwhile to mention that the Au layer thickness is a critical parameter for obtaining high sensitivity

of the SPR sensor due to the angular shape of the reflectance. The deeper and sharper curve leads to increased sensitivity.

It is noted that the reflectivity of the SPR curve and the energy transfer are in reverse proportion. This means that the lower the reflectance is, the larger the energy transfer. The energy transfer reaches a maximum value as the thickness of the Au layer approaches 40 nm, as shown in Figure 3(b), leading to the strongest SPR excitation.

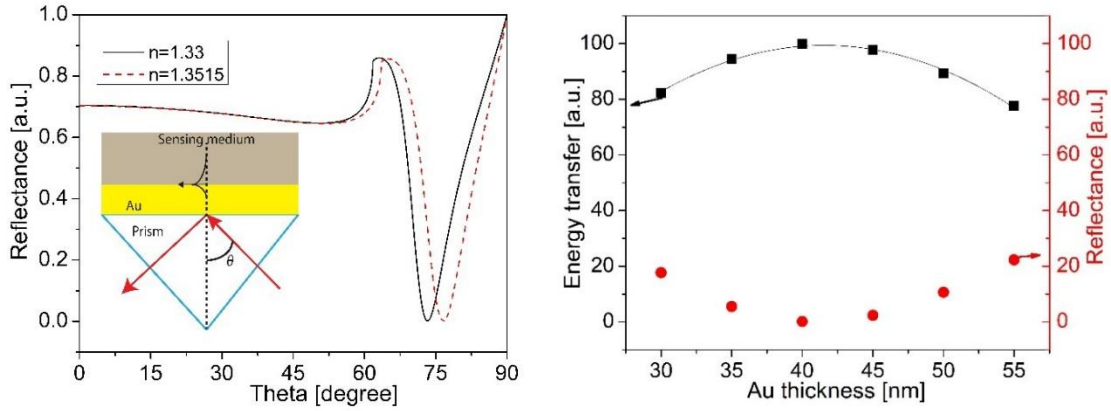

(a) (b)

Figure 3. a) The change in resonance condition for different RI of the sensing medium; b) The relation between reflectance and energy transfer

A parabolic curve was used to fit a quadratic second-order equation $E_T = ad_{Au}^2 + bd_{Au} - E_o$ to the simulated data in Figure 3(b) to find the ideal characteristic shape for energy transfer based on the change in the thickness of the Au layer. The results show that the minimum energy transfer (E_o) was estimated at 115.11 a.u.. The optimal thickness of Au was obtained at 40 nm, corresponding to 99.86 a.u. of energy transfer. Moreover, the correlation coefficient (R^2) was higher than 0.99, indicating that the proposed second-order quadratic model fits the data well (Table 2).

Table 2. Kinetic parameters in energy transfer

Wavelength (nm)	Minimum energy transfer Eo (a.u.)	Fitting coefficients		
		a	b	R2
632.8 nm	115.11	-0.12	10.32	0.99

Based on the above results, an Au thickness of 40 nm was used to estimate the sensor sensitivity, detection accuracy, and penetration depth. In this simulation, the refractive index (RI) of the sensing medium was set in the range 1.3300-1.3515 (RIU). When the RI of the sensing medium increases, the SPR curves shift toward higher incident angles, as shown in Figure 3(a). The sensor sensitivity is estimated based on the equation given below (Chien et al., 2007).

$$S = \frac{\delta\theta}{\delta n} \tag{15}$$

where S is the sensor sensitivity, n is RI of the sensing medium, and θ is the incident angle of the laser light. The sensor sensitivity was estimated at 154.4°/RIU for the Au layer thickness of 40 nm based on Equation (15).

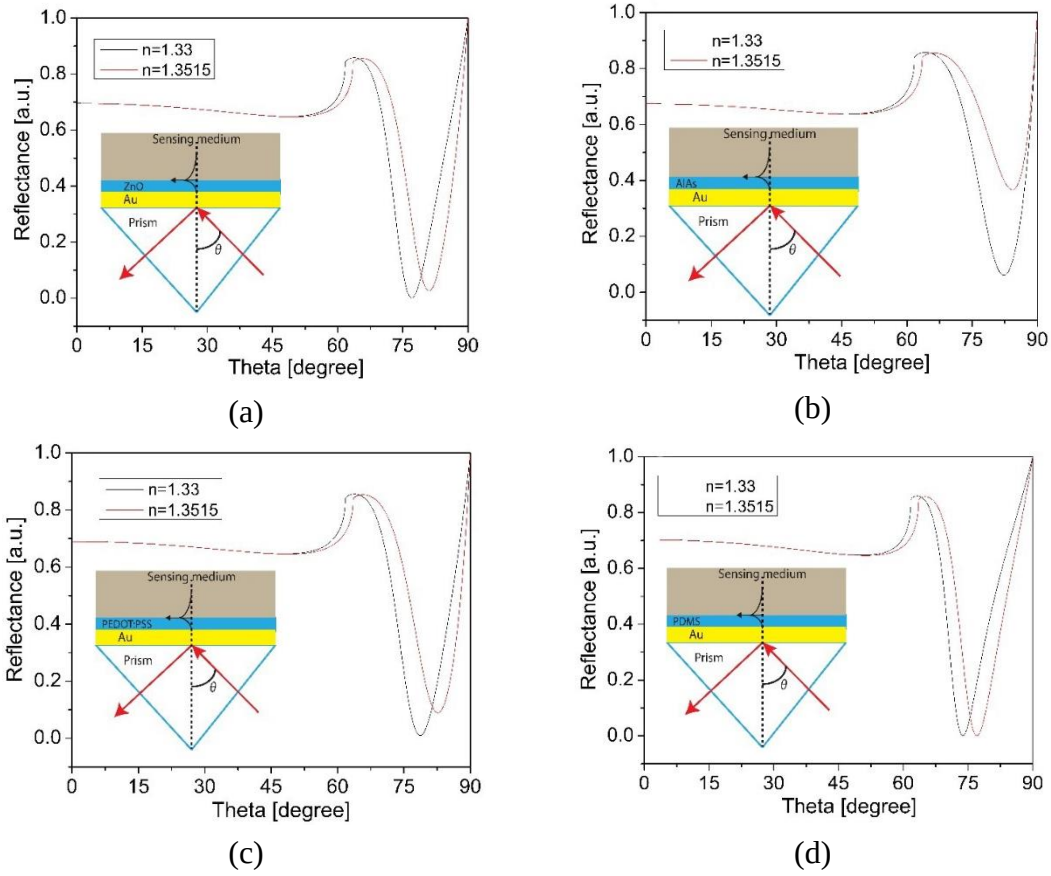

Figure 4. Different combinations of materials for the change in resonance condition

Note: a) ZnO of 5 nm thickness; b) AlAs of 5 nm thickness; c) PEDOT:PSS of 5 nm thickness; d) PDMS of 5 nm thickness.

For enhancement of the sensor sensitivity, combinations of Au and additional materials (AlAs, PEDOT:PSS, ZnO, and PDMS) were investigated. The 5-nm thickness of the additional materials was combined with the Au of 40-nm thickness to form the sensor structure of prism/Au/additional layer/sensing medium. The sensor sensitivity was found by changing the refractive index of the sensing medium in the range from 1.3300-1.3515 RIU, which corresponds to a change of *Escherichia coli* concentration of 10^3 cfu.mL (Liu et al., 2016). As shown in Figure 4, the SPR characteristic shape was shifted when the refractive index increased. The sensor sensitivity was estimated at 90.70, 186.07, 185.11, and 150.69°/RIU for the case of Au/AlAs, Au/PEDOT:PSS, ZnO, and PDMS, respectively. The highest sensitivity was obtained from the combination of Au and PEDOT:PSS with a thickness ratio of 40:5 nm. This result is comparable with the

case of Au/ZnO, as shown in Figure 5. The high sensitivity was caused by the small value of the imaginary part of the dielectric constant of PEDOT:PSS. In addition, this sensitivity was 1.2 times higher than the case of using only the Au layer. The smaller the imaginary part of the dielectric constant is, the greater the sensitivity.

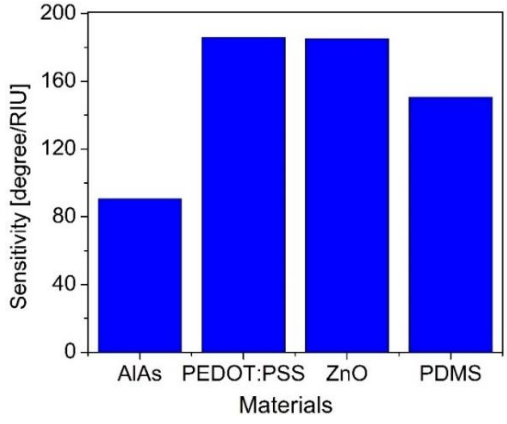

Figure 5. Sensor sensitivity based on an Au layer combined with different materials

The combination of Au with an additional material, such as AlAs, PEDOT:PSS, ZnO, and PDMS, for the SPR sensor with an operational wavelength of 633 nm offers several advantages. The sensitivity of the sensor based on the combination of Au/PEDOT:PSS is higher than the sensor using only expensive materials like Au. The operating refractive index range of 0.0215 RIU corresponds to a change in *E. coli* concentration of 10^3 cfu.mL, indicating that the proposed sensor with the combination of Au and PEDOT:PSS can be applied for the detection of small concentrations of *E. coli*.

4. CONCLUSION

This paper presents simulation results for an SPR optical sensor having a layer of Au and an additional layer of another material, AlAs, PEDOT:PSS, ZnO, or PDMS, with an operating wavelength of 632.8 nm. The results show that the optimal combination consists of Au and PEDOT:PSS layers with thicknesses around 40 nm and 5 nm, respectively. This combination offers a sensor sensitivity of 186.07°/RIU, which is 1.2 times better than the sensor using only an Au layer. The research results offer the advantage of using a combination of Au/PEDOT:PSS for SPR excitation and detection of large biomolecules in small concentrations.

ACKNOWLEDGEMENT

This research is funded by the Vietnam National Foundation for Science and Technology Development (NAFOSTED) under grant number 103.03-2018.351.

REFERENCES

Akter, S., & Razzak, S. M. A. (2019). Highly sensitive open-channels based plasmonic biosensor in visible to near-infrared wavelength. *Results in Physics, 13,* 1-8.

Chah, S. W., Yi, J. H., & Zare, R. N. (2004). Surface plasmon resonance analysis of aqueous mercuric ions. *Sensors and Actuators B: Chemical*, *99*(2-3), 216-222.

Chen, C. W., Hsiao, S. Y., Chen, C. Y., Kang, H. W., Huang, Z. Y., & Lin, H. W. (2015). Optical properties of organometal halide perovskite thin films and general device structure design rules for perovskite single and tandem solar cells. *Journal of Materials Chemistry A*, *3*(17), 9152-9159.

Chien, F. C., Lin, C. Y., Yih, J. N., Lee, K. L., Chang, C. W., Wei, P. K., Sun, C. C., & Chen, S. J. (2007). Coupled waveguide-surface plasmon resonance biosensor with subwavelength grating. *Biosensors and Bioelectronics*, *22*(11), 2737-2742.

Fen, Y. W., Yunnus, W. M. M., & Talib, Z. A. (2015). Analysis of Pb(II) ion sensing by crosslinked chitonsan thin film using surface plasmon resonance spectroscopy. *Optik*, *124*(2), 126-133.

Gupta, V., Probst, P. T., Goβler, F. R., Steiner, A. M., Schubert, J., Brasse, Y., & Konig, T. A. F. (2019). Mechanotunable surface lattice resonances in the visible optical range by soft lithography templates and directed self-assembly. *ACS Applied Material Interfaces*, *11*(31), 28189-28196.

Ho, H. P., Lam, W. W., & Wu, S. Y. (2002). Surface plasmon resonance sensor based on the measurement of differential phase. *Review of Scientific Instruments, 73*(10), 3534-3539.

Homola, J. (1995). Optical fiber sensor based on surface plasmon excitation. *Sensors and Actuators B: Chemical*, *29*(1), 401-405.

Iga, M., Seki, A., & Watanabe, K. (2004). Hetero-core structured fiber optic surface plasmon resonance sensor with silver film. *Sensors and Actuators B-Chemical, 101*(3), 368-372.

Jorgenson, R. C., & Yee, S. S. (1993). A fiber-optic chemical sensor based on surface plasmon resonance. *Sensors and Actuators B: Chemical*, *12*(3), 213-220.

Liu, P. Y., Chin, L. K., Ser, W., Chen, H. F., Hsieh, C. M., Lee, C. H., Sung, K. B., Ayi, T. C., Yap, P. H., Liedberg, B., Wang, K., Bourouina, T., & Leprince-Wang, Y. (2016). Cell refractive index for cell biology and disease diagnosis: past, present and future. *Lab on a Chip, 16*(4), 634-644.

Maharana, P. K., & Jha, R. (2012). Chalcogenide prism and graphene multilayer based surface plasmon resonance affinity biosensor for high performance. *Sensors and Actuators B-Chemical*, *169*(5), 161-166.

McPeak, K. M., Jayanti, S. V., Kress, S. J. P., Meyer, S., Lotti S., Rossinelli, A., & Norris, D. J. (2015). Plasmonic films can easily be better: Rules and recipes. *ACS Photonics*, *2*(3), 326-333.

Mishra, A. K., Mishra, S. K., & Gupta, B. D. (2015). SPR based fiber optic sensor for refractive index sensing with enhanced detection accuracy and figure of merit in visible region. *Optics Communications, 344*(1), 86-91.

Nguyen, T. T., Lee, E. C., & Ju, H. (2014). Bimetal coated optical fiber sensors based on surface plasmon resonance induced change in birefringence and intensity. *Optics Express*, *22*(5), 5590-5598.

Nguyen, T. T., Bea, S. O., Kim, D. M., Yoon, W. J., Park, J. W., An, S. S., & Ju, H. (2015). A regenerative fiber optic sensor using surface plasmon resonance for clinical diagnosis of fibrinogen. *International Journal of Biomedicine, 10*, 155-163.

Nguyen, T. T., Trinh, K. T. L., Yoon, W. J., Lee, N. Y., & Ju, H. (2017). Integration of a microfluidic polymerase chain reaction device and surface plasmon resonance fiber sensor into an inline all-in-one platform for pathogenic bacteria detection. *Sensors and actuators B: Chemical*, *242*, 1-8.

Otto, A. (1968). Excitation of nonradiative surface plasma waves in silver by the method of frustrated total reflection. *Zeitschrift fur Physik*, *216*(4), 398-410.

Palumbo, M., Pearson, C., Nagel, J., & Petty, M. C. (2003). Surface plasmon resonance sensing of liquids using polyelectrolyte thin films. *Sensors and Actuators B: Chemical, 91*(1-3), 291-297.

Panta, Y. M., Liu J., Cheney, M. A., Joo, S. W., & Qian, S. (2009). Ultrasensitive detection of mercury (II) ions using electrochemical surface plasmon resonance with magnetohydrodynamic convention. *Journal of Colloid and Interface Science*, *333*(2), 485-490.

Patnaik, A., Senthilnathan, K., & Jha, R. (2015). Graphene based conducting metal oxide coated D-shaped optical fiber SPR sensor. *IEEE Photonics Technology Letters*, *27*(23), 2437-2440.

Prabowo, B. A., Purwidyantri, A., & Liu, K. C. (2018). Surface plasmon resonance optical sensor: A review on light source technology. *Biosensors, 8*(3), 1-27.

Raether, H., & Kretschmann, E., (1968). Radiative decay of non radiative surface plasmons excited by light. *Zeitschrift fur Naturforschung A*, *23*(a), 2135-2136.

Rakic, A. D., & Majewski, M. L. (1996). Modeling the optical dielectric function of GaAs and AlAs: Extension of Adachi's model. *Journal of Apllied Physics, 80*(10), 5909-5914.

Sharmal, A. K., & Mohr, G. J. (2008). On the performance of surface plasmon resonance based fibre optic sensor with different bimetallic nanoparticle alloy combinations. *Journal of Physics D: Applied Physics*, *41*, 1-7.

Srivastava, S. K., Verma, R., & Gupta, B. D. (2016). Theoretical modeling of a self-referenced dual mode SPR sensor utilizing indium tin oxide film. *Optics Communications, 369*, 131-137.

Stelling, C., Singh, C. R., Karg, M., Konig, T. A., Thelakkat, M., & Retsch, M. (2017). Plasmonic nano meshes: their ambivalent role as transparent electrodes in organic solar cells. *Science Reports*, *7*, 1-13.

Telezhnikova, O., & Homola, J. (2006). New approach to spectroscopy of surface plasmons. *Optics Letters*, *31*(22), 3339-3341.

Truong, T. V. N., Tran, T. N. H., Nam, E., Nguyen, T. T., Yoon, W. J., Cho, S., Kim, J., Chang, K. A., & Ju, H. (2018). Blood-based immunoassay of tau proteins for early diagnosis of Alzheimer's disease using surface plasmon resonance fiber sensors. *RSC Advance*, *8*(14), 7855-7862.

Turker, B., Guner, H., Ayas, S., Ekiz, O. O., Acar, H., Guler, M. O., & Dana, A. (2011). Grating coupler integrated photodiodes for plasmon resonance based sensing. *Lab on a Chip*, *11*(2), 282-287.

Vala, M., Chadt, K., Piliarik, M., & Homola, J. (2010). High-performance compact SPR sensor for multi-analyte sensing. *Sensors and Actuators B: Chemical, 148(2),* 544-549.

Van Gent, J., Lambeck, P. V., Kreuwel, H. J., Gerritsma, G. J., Sudhölter, E. J., Reinhoudt, D. N., & Popma, T. J. (1990). Optimization of a chemooptical surface plasmon resonance based sensor. *Applied Optics*, *29*(19), 2843-2849.

Wu, S. Y., Ho, H. P., Law, W. C., Lin, C., & Kong, S. K. (2004). Highly sensitive differential phase-sensitive surface plasmon resonance biosensor based on the Mach–Zehnder configuration. *Optics Letters, 29*(20), 2378-2380.

Yang, D., Lu, H. H., Chen, B., & Lin, C. W. (2010). Surface plasmon resonance of SnO_2/Au Bi-layer films for gas sensing applications. *Sensors and Actuators B: Chemical*, *145*(2), 832-838.

Yuan, W., Ho, H. P., Wong, C. L., Kong, S. K., & Lin, C. (2007). Surface plasmon resonance biosensor incorporated in a Michelson interferometer with enhanced sensitivity. *Sensors Journal*, *7*(1), 70-73.

Yuan, Y., Wang, L., & Huang, J. (2012). Theoretical investigation for two cascaded SPR fiber optic sensors. *Sensors and Actuators B: Chemical*, *161*(1), 269-273.

Zhao, J., Cao, S., Liao, C., Wang, Y., Wang, G., Xu, X., Fu, C., Xu, G., Lian, J., & Wang, Y. (2016). Surface plasmon resonance refractive sensor based on silver-coated side-polished fiber. *Sensors and Actuators B: Chemical, 230*, 206-211.